

ZTF SN Ia DR2: Colour standardisation of Type Ia Supernovae and its dependence on environment

Ginolin, M.^{1,*}, Rigault, M.¹, Copin, Y.¹, Popovic, B.¹, Dimitriadis, G.², Goobar, A.³, Johansson, J.³, Maguire, K.², Nordin, J.⁴, Smith, M.⁵, Aubert, M.⁶, Barjou-Delayre, C.⁶, Burgaz, U.², Carreres, B.^{7,8}, Dhawan, S.⁹, Deckers, M.², Feinstein, F.⁷, Fouchez, D.⁷, Galbany, L.^{10,11}, Ganot, C.¹, de Jaeger, T.¹², Kim, Y.-L.⁵, Kuhn, D.¹², Lacroix, L.^{3,12}, Müller-Bravo, T. E.^{10,11}, Nugent, P.^{13,14}, Racine, B.⁷, Rosnet, P.⁶, Rosselli, D.⁷, Ruppin, F.¹, Sollerman, J.¹⁵, Terwel, J.H.^{2,16}, Townsend, A.⁴, Dekany, R.¹⁷, Graham, M.¹⁸, Kasliwal, M.¹⁸, Groom, S.L.¹⁹, Purdum, J.¹⁷, Rusholme, B.¹⁹, and van der Walt, S.²⁰

- ¹ Univ Lyon, Univ Claude Bernard Lyon 1, CNRS, IP2I Lyon/IN2P3, UMR 5822, F-69622, Villeurbanne, France
- ² School of Physics, Trinity College Dublin, College Green, Dublin 2, Ireland
- ³ Oskar Klein Centre, Department of Physics, Stockholm University, SE-10691 Stockholm, Sweden
- ⁴ Institut für Physik, Humboldt Universität zu Berlin, Newtonstr 15, 12101 Berlin, Germany
- ⁵ Department of Physics, Lancaster University, Lancs LA1 4YB, UK
- ⁶ Université Clermont Auvergne, CNRS/IN2P3, LPCA, F-63000 Clermont-Ferrand, France
- ⁷ Aix Marseille Université, CNRS/IN2P3, CPPM, Marseille, France
- ⁸ Department of Physics, Duke University, Durham, NC 27708, USA
- ⁹ Institute of Astronomy and Kavli Institute for Cosmology, University of Cambridge, Madingley Road, Cambridge CB3 0HA, UK
- ¹⁰ Institute of Space Sciences (ICE, CSIC), Campus UAB, Carrer de Can Magrans, s/n, E-08193, Barcelona, Spain
- ¹¹ Institut d'Estudis Espacials de Catalunya (IEEC), E-08034 Barcelona, Spain
- ¹² Sorbonne Université, CNRS/IN2P3, LPNHE, F-75005, Paris, France
- ¹³ Lawrence Berkeley National Laboratory, 1 Cyclotron Road MS 50B-4206, Berkeley, CA, 94720, USA
- ¹⁴ Department of Astronomy, University of California, Berkeley, 501 Campbell Hall, Berkeley, CA 94720, USA
- ¹⁵ Oskar Klein Centre, Department of Astronomy, Stockholm University, SE-10691 Stockholm, Sweden
- ¹⁶ Nordic Optical Telescope, Rambla José Ana Fernández Pérez 7, ES-38711 Breña Baja, Spain
- ¹⁷ Caltech Optical Observatories, California Institute of Technology, Pasadena, CA 91125
- ¹⁸ Division of Physics, Mathematics, and Astronomy, California Institute of Technology, Pasadena, CA 91125, USA
- ¹⁹ IPAC, California Institute of Technology, 1200 E. California Blvd, Pasadena, CA 91125, USA
- ²⁰ Berkeley Institute for Data Science, University of California Berkeley, Berkeley, CA 94720, USA

Received;

ABSTRACT

Context. As Type Ia supernova cosmology transitions from a statistics dominated to a systematics dominated era, it is crucial to understand leftover unexplained uncertainties affecting their luminosity, such as the ones stemming from astrophysical biases. Indeed, Type Ia supernovae are standardisable candles, whose absolute magnitude reach a typical 0.15 mag scatter once empirical correlations with their lightcurve stretch and colour and with properties of their environment are accounted for.

Aims. In this paper, we investigate how the standardisation process of Type Ia supernovae depends on environment, to ultimately reduce their scatter in magnitude, focusing on colour standardisation.

Methods. We use the volume-limited ZTF SN Ia DR2 sample, which offers unprecedented statistics for the low redshift ($z < 0.06$) range. We first study the colour distribution, focusing on the effects of dust, to then select a dustless subsample of objects originating from low stellar mass environments and from the outskirts of their host galaxies. We then look at the colour-residuals relation and its associated parameter β . Finally, we investigate the colour dependency of the environment-dependent magnitude offsets (steps), to try to disentangle intrinsic and extrinsic colour origin.

Results. Our sample of nearly 1,000 supernovae probes well the red tail of the colour distribution, up to $c = 0.8$. The dustless sample exhibits a significantly lower red tail (4.6σ) in comparison to the whole sample, but both samples have similar distributions around $c \sim 0$. This suggests that reddening above $c \geq 0.2$ is dominated by host interstellar dust absorption while the rest of the colour scatter is of intrinsic origin. Looking at the colour-residuals relation, we find it to be linear with lightcurve colour. We show hints of a potential evolution of β with host stellar mass at a 2.5σ level. Finally, unlike recent claims from the literature, we see no evolution of steps as a function of lightcurve colour, suggesting that dust may not be the dominating mechanism responsible for the environmental dependency of Type Ia supernovae magnitude.

Key words. Cosmology: dark energy – supernovae: general

1. Introduction

Type Ia supernovae (SNe Ia) were the tools that made possible the discovery of the accelerated expansion of the Universe, due

* Corresponding author: m.ginolin@ip2i.in2p3.fr

to their standardisable nature (Riess et al. 1998; Perlmutter et al. 1999). They are still a crucial probe for precision cosmology, especially in the determination of the dark energy equation of state parameter w (Planck Collaboration 2020; Brout et al. 2021) and of the Hubble-Lemaître constant H_0 (Freedman 2021; Riess et al. 2022), as they are a unique tracer of the local Universe expansion.

The raw observed magnitudes of SNe Ia exhibits a scatter of ~ 0.4 mag. Part of this scatter can be reduced thanks to empirical relations discovered in the mid-90s, between SN magnitudes and their colour, and between SN magnitudes and their stretch (Phillips 1993; Tripp 1998). Using these relations, the scatter can go down to around ~ 0.15 mag, the residual scatter being dominated by a scatter dubbed intrinsic, for lack of better understanding. In the mid-2010s, an extra standardisation relation between SN host mass and their magnitude was brought to light (Kelly et al. 2010; Sullivan et al. 2010; Lampeitl et al. 2010; Childress et al. 2013), accounting for astrophysical biases on SN Ia luminosity. Contrary to the stretch and colour magnitude relations, which are linear, this correction has usually been parameterised as a magnitude offset between high mass and low mass hosts, named the "mass step".

While widely used in cosmology, the formation mechanism of SNe Ia is still unclear. Type Ia SNe are thought to be the thermonuclear explosion of a Carbon-Oxygen white dwarf. However, several scenarios coexist in the literature (see Maeda & Terada 2016 for a review): e.g., the single degenerate scenario, where a white dwarf accretes enough material from a companion star to reach masses high enough to reach instability regimes, or the double degenerate scenario, where explosion occurs after a merger of two white dwarfs or the accretion of one white dwarf by the other. The lack of understanding of this mechanism, both theoretically or through first principle numerical simulations, also means that the link between SN Ia properties and their environments is largely unknown. Host stellar mass, stellar age, gas and stellar metallicities and/or star-formation rate might play various roles in SN Ia observational characteristics, but it is unclear to what extent.

In that context, the origin of SN Ia colour, whose correlation with magnitude provides the strongest scatter reduction in the standardisation process, is particularly discussed. Current interpretations suggest that it is a mixture of intrinsic colour resulting from the poorly understood formation mechanisms and additional reddening by line of sight host interstellar dust (e.g. Jha et al. 2007; Mandel et al. 2017; Uddin et al. 2020; Brout & Scolnic 2021; Johansson et al. 2021; Kelsey et al. 2023). Yet, usual SN Ia standardisation assumes a unique linear colour-magnitude relation coefficient β , which might not correctly describe the data if indeed the colour origin is twofold. Furthermore, this single β coefficient is found to be significantly lower than what would be expected from nearby galaxy dust models and data (Wang 2005; Nobili & Goobar 2008; Goobar 2008; Amanullah et al. 2015; Salim et al. 2018).

In parallel, stretch and colour standardised SN Ia magnitudes exhibit a significant dependency with the SN host properties, such that SNe Ia from massive, red and/or passive galaxies are significantly fainter than those from low mass, blue and/or star forming environments (e.g. Hamuy et al. 1996; Sullivan et al. 2010; Childress et al. 2013; Rigault et al. 2013; Kim et al. 2018; Rigault et al. 2020; Kelsey et al. 2021). Yet, the exact origin of these magnitude "steps" is highly debated, though, for historical reason and simplicity, the "mass step" is the one commonly used in current cosmological analyses (Betoule et al. 2014; Scolnic et al. 2018; Brout et al. 2021; Riess et al. 2022). Two explana-

tions are currently the focus of discussions. The first supposes an intrinsic origin of the environmental magnitude offset related to the progenitor "age", in a sense of a prompt vs. delayed dichotomy (e.g. Sullivan et al. 2006), so that prompt SNe Ia are intrinsically fainter after stretch and colour standardisation than delayed ones (Rigault et al. 2013, 2020; Briday et al. 2021). Alternatively, interstellar dust may vary as a function of the environments, such that massive hosts have at the same time more dust and different dust properties than low mass hosts (Brout & Scolnic 2021; Popovic et al. 2021). Most recent cosmological results (Brout et al. 2021; Riess et al. 2022) assume the latter (see Popovic et al. 2023, and references therein). In practice, both effects are likely to play a role, and the question will then be the relative amplitude of each one (Wiseman et al. 2022; Kelsey et al. 2023).

An avenue to solve this question is to investigate the environmental dependency of SNe Ia observed in the near infrared, where the influence of dust should be negligible (Jones et al. 2022; Galbany et al. 2022) and SN Ia magnitudes naturally less scattered (e.g. Barone-Nugent et al. 2012; Dhawan et al. 2018). Were the environmental magnitude offsets solely due to varying dust properties, NIR data should not exhibit any mass step. Yet, Uddin et al. (2020) and Ponder et al. (2021) do report significant steps, with similar amplitudes than those found using optical data, strongly disfavoring the dust scenario. However, Johansson et al. (2021) and Jones et al. (2022) have more mitigated results, also finding steps, but not as significant ($\sim 2\sigma$ level), suggesting indeed that NIR SN Ia data might not suffer from the aforementioned environmental biases.

In this paper, we investigate in detail the colour part of SN Ia standardisation using the second data release of the Zwicky Transient Facility (ZTF, Bellm et al. 2019; Graham et al. 2019; Masci et al. 2019; Dekany et al. 2020) cosmology group (SN Ia DR2, Rigault et al., 2024a, Smith et al. 2024). A companion paper (Ginolin et al. 2024a) focuses on stretch standardisation, as well as on the usual magnitude offsets correcting for environment dependence (steps). In that paper, using a $\mathcal{O}(1000)$ volume limited SN Ia dataset, we show that the stretch distribution follows what was expected by the "prompt and delayed" model from Rigault et al. (2020) and Nicolas et al. (2021), and that ZTF exhibits a large environmental bias (≥ 0.15 mag). In this paper, we investigate the origin of this step in the context of the age vs. dust discussion.

After a quick introduction of the ZTF DR2 data in Section 2, we first study the ZTF SN Ia colour distribution and its dependency with SN environment in Section 3. In Section 4, we then look at the host dependency of the colour standardisation parameter β . In that section, we discuss the linearity of the colour-magnitude relation in the context of the twofold origin of SN colour. The origin of the SN Ia magnitude astrophysical dependency is studied in Section 5, where we analyse how magnitude offsets vary as a function of SN colour. We finally discuss the robustness of our results and their consequences for SN Ia cosmology in Section 6. We conclude in Section 7.

2. Data

2.1. Zwicky Transient Facility SN Ia DR2

In this paper, we use the ZTF SN Ia DR2 sample described in Rigault et al. (2024a). The ZTF DR2 data are presented in details in Smith et al. (2024). In this analysis, we aim at probing the properties of the underlying SNe Ia population, and we therefore

limit our sample to well measured objects in the volume-limited redshift range ($z < 0.06$).

As described in Rigault et al. (2024a), these well measured SNe Ia are those passing the following quality cuts: (1) At least seven 5σ detections, two pre-, two-post maximum light and in two different filters, only considering the rest-frame phase range $[-10 \text{ days}, +40 \text{ days}]$ used to fit the SALT2 parameters (Guy et al. 2010; Betoule et al. 2014; Taylor et al. 2021) (2) A SALT2 lightcurve fit probability greater than 10^{-7} . We fit the ZTF lightcurves with the SALT2 ‘‘T21’’ model (Taylor et al. 2021), accounting for Milky Way extinction (see details in Smith et al. 2024). We limit our targets to those having the following SALT2 parameters: $c \in [-0.2, 0.8]$, with $\sigma_c < 0.1$, $x_1 \in [-3, +3]$, with $\sigma_{x_1} < 1$ and a peak-luminosity date t_0 measured with a precision of 1 day or less, leaving 970 SNe Ia. As recommended by Rose et al. (2022), we extend the colour range above the usual $c < 0.3$, which allows us to probe the characteristics of the full SN Ia colour distribution. In addition, we remove ~ 20 peculiar SNe Ia (e.g. 91bg or Ia-CSM), but we keep edge cases such as 91T-like, as they are not usually identifiable by higher redshift samples (see details in Dimitriadis et al. 2024). We show in Sect. 6.1 that our results do not depend on these cuts. We also remove ~ 40 additional objects with no host-property measurements, leaving 927 SNe Ia. Finally, to be consistent throughout the analysis, we remove an additional 7 objects (0.1%), which get discarded by the outlier rejection in the Hubble residual standardisation (see Sect. 4).

Our final sample therefore contains 920 SNe. In this sample, 75% SNe have a redshift coming from host spectroscopic features with a typical precision greater than $\sigma_z \leq 10^{-4}$. The remaining 25% have a redshift coming from SN spectroscopic features. As detailed in Smith et al. (2024), these redshifts are unbiased and have a typical precision of $\sigma_z \leq 3 \times 10^{-3}$.

2.2. Environmental cuts.

To study SN Ia environmental dependency, we use four optical photometric tracers made available as part of the SN Ia DR2: local (2-kpc radius) and global PS1 .g-PS1 .z colour (Chambers et al. 2016) and local and global stellar mass (see details in Smith et al. 2024). Both colours and photometric masses have been corrected for Milky Way extinction. When compared, the SNe Ia are split in subsamples following these cuts:

- $(g - z)_{\text{local,global}}^{\text{cut}} = 1$, which corresponds the gap in the colour distribution.
- $\log(M_\star/M_\odot)_{\text{global}}^{\text{cut}} = 10$, as usual in the literature.
- $\log(M_\star/M_\odot)_{\text{local}}^{\text{cut}} = 8.9$, the median of the local mass distribution.

3. Colour distribution

In this section, we investigate the SN colour (c) distribution.

The SALT2 (‘‘T21’’, Taylor et al. 2021) colour distribution of the sample used in this analysis is shown in Fig. 1. There is a clear asymmetry visible in this distribution, with a tail extending redward, as pointed out by Brout & Scolnic (2021) for a different compilation of SNe Ia.

Following former modelling (e.g. Jha et al. 2007; Mandel et al. 2011, 2017), we model the colour distribution as the convolution of a normal distribution $\mathcal{N}(c | c_{\text{int}}, \sigma_c)$ with an exponential decay for positive colour, such that:

$$P(c) = \mathcal{N}(c | c_{\text{int}}, \sigma_c) \otimes \begin{cases} 0 & \text{if } c \leq 0 \\ \frac{1}{\tau} e^{-c/\tau} & \text{if } c > 0 \end{cases} \quad (1)$$

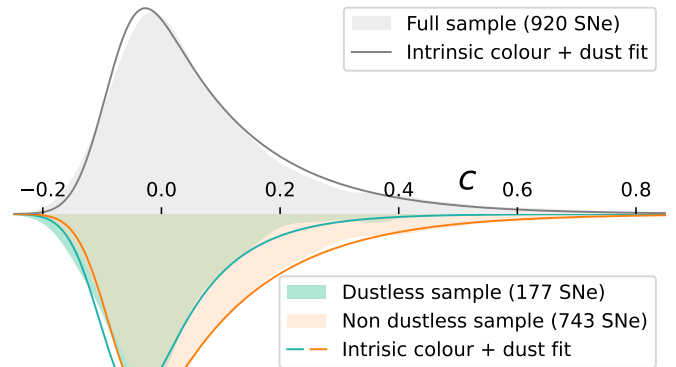


Fig. 1. Ideogram of SN colour, along with the fit described in Eq. 1, for the full sample (top plot), and for the ‘‘dustless’’ and ‘‘non dustless’’ samples (bottom plot). The mean error on c is added in quadrature to σ_c in the plotted fits, as we take into account errors on c in our model.

Table 1. Best fitted values for the parameters of Eq. 1, for the full sample and the dustless/non dustless samples defined in Sect. 3.

Sample	c_{int}	σ_c	τ
Full sample	-0.086 ± 0.004	0.029 ± 0.005	0.157 ± 0.007
Dustless sample	-0.092 ± 0.008	0.032 ± 0.008	0.099 ± 0.011
Non dustless sample	-0.081 ± 0.005	0.029 ± 0.006	0.168 ± 0.008

Conceptually, the normal distribution should represent the intrinsic SN Ia colour scatter, while the exponential decay accounts for additional reddening due to the host galaxy interstellar dust. We evaluate $P(c_i)$ from Eq. 1 for the i^{th} SN and then minimise $\sum_i -\log(P(c_i))$ with `iminuit` (Dembinski & et al. 2020), adding the measurement errors on c in quadrature with σ_c .

The best fitted model for the ZTF data is shown in Fig. 1, and the values of the parameters are presented in Table 1. It qualitatively reproduces well the data, supporting the idea of an intrinsic and extrinsic origin of the observed SN Ia colours.

To further investigate our physical interpretation of the model, we split our sample along various environmental properties. If indeed intrinsic, the Gaussian parameters c_{int} and σ_c should be independent of environment, while the dust-related parameter τ should become insignificant in dust free environments.

We choose five parameters to characterise the SN Ia environment, all described in Sect. 2.1: colour ($g - z$) (local and global), stellar mass (local and global) and the dimensionless Directional Light Ratio (dDLR, Sullivan et al. 2006; Gupta et al. 2016). We then fit the subsamples in two ways:

1. Fitting the full model on each subsample. This allows us to assess if c_{int} and σ_c vary as a function of the environment.
2. Fitting only τ per subsample, while keeping the supposedly intrinsic distribution parameters (c_{int}, σ_c) fixed to the values of the full sample (as done in Brout & Scolnic 2021).

The resulting fitted parameters are shown in Fig. 2. As illustrated in this figure, c_{int} and σ_c appear to be independent from environment. The sole visible variation is the redder average colour c_{int} of SNe Ia from locally massive environments (2.6σ). But, accounting for the look elsewhere effect (LEF, 15 trials, $\Delta c_{\text{int}}, \Delta \sigma_c$ and $\Delta \tau$ in five environmental splits), this variation is only at the 1.5σ level. We thus conclude that c_{int} and σ_c are independent

from environment, reinforcing the claim that they correspond to an intrinsic SN Ia colour distribution.

The τ parameter, however, does vary as a function of the environment. SNe Ia in the outskirts of their host galaxy (dDLR > 1.5) or in low stellar mass regions display significantly lower τ values than those in the center of their galaxy or in locally massive environments (respectively 4.1σ and 5.8σ , or 3.4σ and 5.3σ when accounting for LEF). This is in accordance with the literature (e.g. Galbany et al. 2012). These variations are not as pronounced when using global properties or using local colour ($\leq 3\sigma$). Such findings support the claim that reddening parameterised by the exponential decay parameter τ is caused by interstellar dust extinction, since galaxy cores and denser environments are significantly dustier than others (see Sect. 6.2 for a discussion on dust in galaxies).

We then define a “dustless” SNe Ia sample of 177 objects, that are both in locally low stellar mass regions and in the outskirts of their host galaxy, following the cuts in Fig. 2. With these cuts, significant host dust extinction along the line of sight of these SNe Ia is unlikely. In contrast, SNe Ia not in this sample may be reddened by dust, though not all will be. The colour distribution for each subsample, as well as the fitted model, are shown in the bottom of Fig. 1. The strong difference between the τ parameters for the dustless and non dustless samples (5.1σ , see Table 1) is clearly visible in Fig. 1. SNe Ia from the “dustless” sample have a much reduced red tail in contrast to other SNe Ia and an apparent mode shift resulting from the reduction of the non-centered exponential decay convolution in Eq. 1. Yet, the c distribution is not purely Gaussian, suggesting that, even if the dust reddening is significantly reduced, it still exists. This is expected since dust does exist in low mass regions or in the edges of galaxies, even if less present. Another consequence of this model is that colours redder than $c > 0.2$ seem largely dominated by host reddening.

4. Colour-residuals relation

In this section, we analyse the environmental dependency and linearity of SN Ia colour standardisation. This section is the colour counterpart of the stretch-standardisation study of Ginolin et al. (2024a), which provides a full description the standardisation procedure in their Section 4. We briefly describe here the key elements.

We compute the Hubble residuals, $\Delta\mu = \mu_{\text{obs}} - \mu_{\text{cosmo}}$, assuming Planck Collaboration (2020) cosmology. For a volume-limited sample like ours, the observed distance moduli can be written as (Tripp 1998):

$$\mu_{\text{obs}} = m_B - M_0 - \beta c + \alpha x_1 - \gamma p \quad (2)$$

with c (colour), x_1 (stretch) and m_B (peak magnitude in B band) estimated per SN using the SALT2 “T21” lightcurve fitter (Guy et al. 2010; Betoule et al. 2014; Taylor et al. 2021). The p term is the probability for a given SN Ia to belong to a given environmental subgroup (e.g. SNe in locally blue environments), and takes into account errors on the environmental proxy used.

The standardisation parameters α , β and γ represent the empirical standardisation relations respectively for stretch, colour and environment. M_0 is the absolute SNe Ia magnitude, degenerate with the Hubble constant. In this paper, we focus on the β standardisation term and its connection with the environmental step (γ). The stretch standardisation parameter (α) as well as the environmental magnitude offset γ are studied in detail in Ginolin et al. (2024a).

We fit the standardisation parameters along with an intrinsic scatter (σ_{int}) using a total- χ^2 fit. As detailed in Ginolin et al. (2024a), this technique, which simultaneously fits for the true underlying x_1 , c and p , outputs unbiased standardisation parameters, unlike the simple χ^2 method that assumes that the measured (and noisy) x_1 , c and p correspond to the truth. This is demonstrated in Section 4 and in the Appendix of Ginolin et al. (2024a) and further illustrated in Appendix A for the β standardisation.

As reported in Ginolin et al. (2024a), we find: $\beta = 3.06 \pm 0.05$, $\alpha = 0.165 \pm 0.010$, $\gamma = 0.157 \pm 0.024$, using local colour as an environmental tracer, for the same sample as the one used in this paper.

In Ginolin et al. (2024a), we identified that the magnitude-stretch relation is significantly non-linear ($> 10\sigma$), with a breaking point near $x_1 \sim -0.5$. To account for this non-linearity, we replace the α term in Eq. 2 by $\mathcal{A}(x_1)$, such that:

$$\mathcal{A}(x_1) = \begin{cases} \alpha_{\text{low}} & \text{if } x_1 < x_1^0 \\ \alpha_{\text{high}} & \text{if } x_1 \geq x_1^0 \end{cases} \quad (3)$$

When accounting for this non-linearity, we find: $\beta = 3.31 \pm 0.02$, $\alpha_{\text{low}} = 0.280 \pm 0.010$, $\alpha_{\text{high}} = 0.088 \pm 0.009$ and $\gamma = 0.185 \pm 0.010$, with $x_1^0 = -0.49 \pm 0.06$. Given the significance of this non-linearity, it appears legitimate to study the colour-magnitude relationship accounting for this discovery. Yet, for the sake of comparison with the literature, we will also perform our analysis using the usual linear α term.

The linearity of the colour-magnitude relation is studied in Sect. 4.1 and its environmental dependency in Sect. 4.2.

4.1. Linearity of the colour-residuals relation

We plot in Fig. 3 the relation between SN colour and Hubble residuals uncorrected for colour, to investigate the linearity of the colour-residuals standardisation relation. This relation appears to be linear in the full colour range $c \in [-0.2, 0.8]$. While consistent with earlier findings (e.g. Rose et al. 2022), such linearity is still surprising given the discussion of the duality of the colour origin discussed in Sect. 3. In that section, we show that bluer SN Ia colours are drawn from an environment-independent Gaussian distribution, while redder colours are likely due to additional interstellar dust reddening, which dominates at $c > 0.2$. Yet, while the physical origin of the colour seems to differ, we do not notice any inflection at high c in Fig. 3, as could be expected if dust and the origin of the intrinsic colour scatter (e.g. temperature) had different colour-magnitude relations. When fitting for two β for two subpopulations split at a fixed cut $c^{\text{cut}} = 0$, no statistically significant deviation appears ($\Delta\beta = -0.60 \pm 0.26$, a 2.2σ significance). This result is in agreement with the literature (e.g. Sullivan et al. 2010; Rigault et al. 2020; Rose et al. 2022) and reassuring for the use of SNe Ia as accurate cosmological distance indicators.

Finally, with $\beta = 3.06 \pm 0.05$ (3.31 ± 0.02 when using broken- α standardisation), which corresponds to an $R_V \sim 2.3$, we confirm that the SN Ia colour law is significantly lower than what would be expected for Milky Way like dust ($R_V \sim 3.1$, see e.g. Goobar 2008).

As illustrated in Fig. 3, our conclusions are not affected if we account for the non-linearity of the stretch-magnitude relation (broken- α).

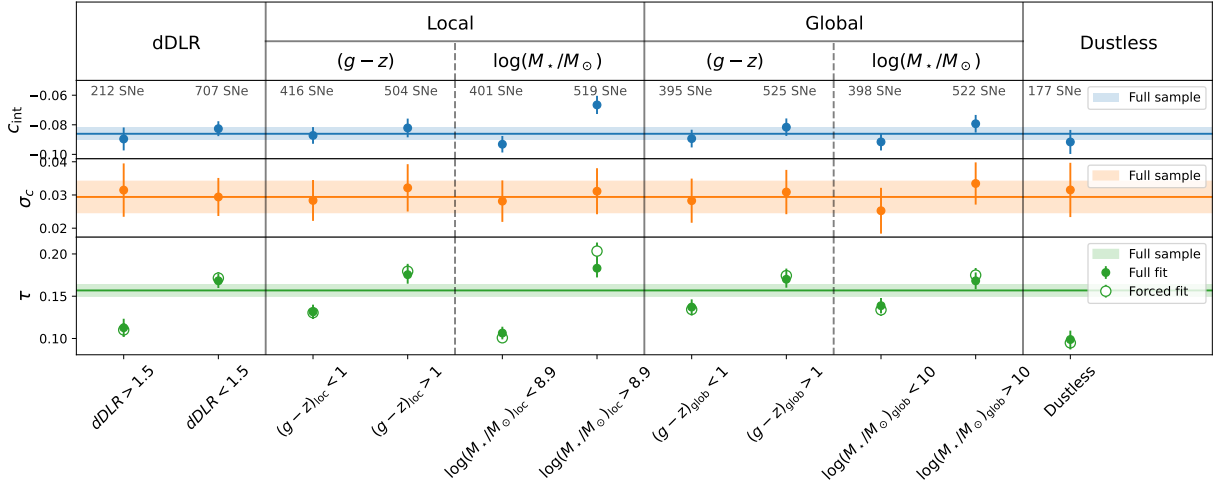


Fig. 2. Parameters for the colour distribution fit described in Eq. 1, for the full sample (shaded bands) as well as for subsamples split on dDLR, environmental colour and stellar mass, both global and local, and the "dustless" sample. The number of SNe in each subsample is indicated on top of the corresponding points. The full points in the bottom plot come from the refitting of the full model (c_{int} , σ_c and τ_{dust}) on the subsample, whereas the empty points correspond to the case where the intrinsic colour distribution is fixed and only the dust distribution is fitted.

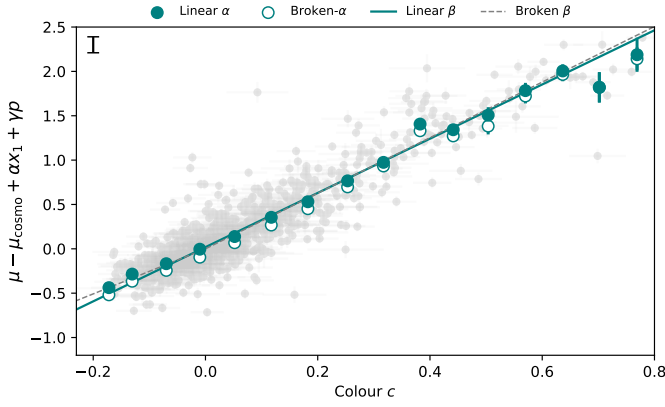


Fig. 3. Binned Hubble residuals (corrected for stretch and environment) versus colour. The errorbars on the points only account for the error on the mean, but a visual indication of the fitted intrinsic scatter is given in the top left corner. The full line is the usual Tripp relation, and the dashed line is the fitted broken- β standardisation. The open points represent the Hubble residuals corrected for stretch using the broken- α standardisation found in Ginolin et al. (2024a).

4.2. β dependence on environment

We further investigate the universality of the colour-magnitude relationship by studying how β varies as a function of the environment.

We split our sample into 6 equally populated bins of global stellar mass containing each $O(150)$ SNe Ia. We then standardise independently each of these bins, i.e. we fit for a set of (α or $(\alpha_{\text{low}}, \alpha_{\text{high}})$), β , M_0 , γ) for each global mass bin. The resulting standardisation parameters are shown in Fig. 4 for the linear stretch standardisation and in Fig. 5 when using the broken- α following Ginolin et al. (2024a). When applying the broken stretch-magnitude relation, we fix the α_{low} and α_{high} at the values fitted on the full sample, since low-mass galaxies do not host any low-stretch SNe Ia (see Ginolin et al., 2024a, or, e.g., Nicolas et al. 2021). To do that, we implement a Gaussian prior centered on the best-fitted values, with a width corresponding to the fitted errors.

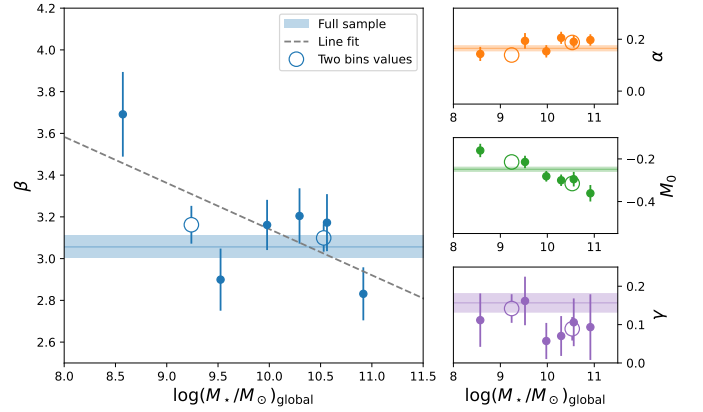


Fig. 4. β , α , M_0 and local colour step γ for each of the global mass bins. The shaded band is the 1σ error around the fitted value for the full sample. The open points are values for when the sample is cut into 2.

Looking at Figs. 4-5, β seems to vary as a function of host stellar mass. With $\beta = 3.69 \pm 0.20$ (linear- α), the lowest bin ($6.6 < \log(M_*/M_\odot) < 9.2$) favors significantly larger β values than higher mass hosts ($\beta = 3.05$ on average for $\log(M_*/M_\odot) \geq 9.2$). Fitting an affine function on the β - $\log(M_*/M_\odot)$ relation in Fig. 4, we find $\beta = (-0.22 \pm 0.09) \times \log(M_*/M_\odot) + (5.4 \pm 0.9)$, with the slope being 2.5σ away from zero. Computing the difference in Akaike Information Criterion (AIC, Burnham & Anderson 2004) between this affine function and a constant, we find $\Delta\text{AIC}=4.2$, meaning that an evolving β is favoured over a constant one. When accounting for the α non-linearity, we find $\beta = (-0.20 \pm 0.08) \times \log(M_*/M_\odot) + (5.1 \pm 0.9)$, the slope being 2.3σ away from 0. In that case, an evolving β is favoured over a constant with $\Delta\text{AIC}=3.4$. Yet, looking at Fig. 4 and Fig. 5, the β - $\log(M_*/M_\odot)$ relation does not look linear, with only the lower mass bin significantly greater than other bins. If we focus on the $\log(M_*/M_\odot) > 9.2$ range, the measured β are consistent with random fluctuation around the average value.

The evolution of the other standardisation parameter is also interesting. For the linear stretch standardisation in Fig. 4, we notice that α slightly shifts towards higher values for higher mass

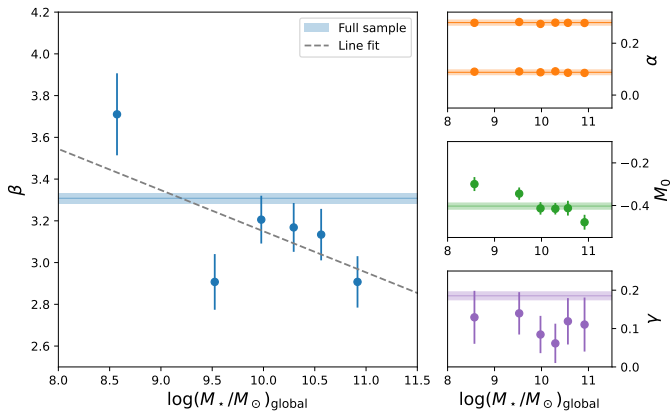


Fig. 5. Same as Fig. 4 but for a broken- α standardisation (Ginolin et al. 2024a). Here a strong prior is imposed on α_{low} and α_{high} , to force them to stay within their errorbars from the full sample.

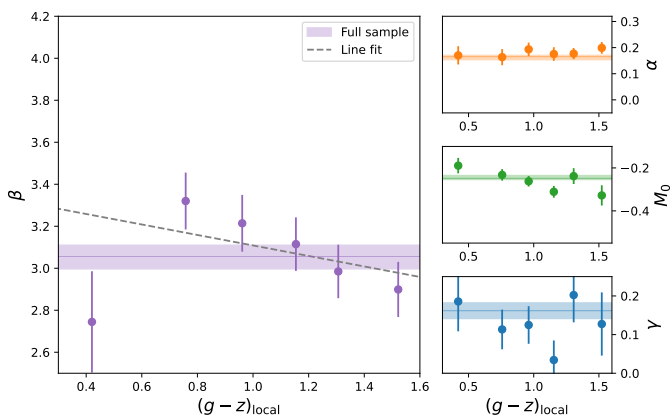


Fig. 6. Same as Fig. 4 but for bins of local colour and a global mass step.

hosts. That is a direct consequence of the non-linearity of the stretch-magnitude relation presented in Ginolin et al. (2024a) and already discussed in their Section 4. Since high-mass hosts favor low-stretch SNe Ia (e.g., Ginolin et al. 2024a, Rigault et al. 2020; Nicolas et al. 2021) and since these have a stronger stretch-magnitude relation than higher stretch SNe Ia, assuming a unique α leads to an increase of the apparent linear coefficient. A detailed modelling of this effect is ongoing and will be the subject of a future publication.

The evolution of the offset term M_0 is also of interest. Despite leaving β free, and while accounting for a colour step per mass bin, the offset term significantly varies with host mass, implying that the mass step is not absorbed by the other terms, as suggested by e.g. Roman et al. (2018); Rigault et al. (2020); Kelsey et al. (2023). Interestingly, the M_0 - $\log(M_*/M_\odot)$ relation does appear linear in Fig. 4 and Fig. 5, with $M_0 = (-0.082 \pm 0.017) \times \log(M_*/M_\odot) + (0.55 \pm 0.17)$.

Finally, when accounting for the non-linearity of the stretch-magnitude relation, clearly demonstrated ($> 14\sigma$) in Ginolin et al. (2024a), the colour step seems stable and independent of the host mass near $\gamma \sim 0.1$, even while allowing for the magnitude offset per bin of mass to change, which absorbs part of the environmental dependencies.

We show a different perspective of this analysis in Fig. 6, where we invert the roles played by local colour and host mass: we split the sample in 6 equally populated bins of local environ-

Table 2. Environmental steps for blue ($c < 0$) and red ($c > 0$) SNe. We here show steps for a linear α and a broken α standardisation (see Sect. 4).

α	Tracer	Blue steps	Red steps
Linear	$(g-z)_{\text{local}}$	0.157 ± 0.033	0.150 ± 0.025
	$\log(M_*/M_\odot)_{\text{global}}$	0.146 ± 0.031	0.168 ± 0.028
Broken	$(g-z)_{\text{local}}$	0.169 ± 0.015	0.163 ± 0.020
	$\log(M_*/M_\odot)_{\text{global}}$	0.157 ± 0.015	0.202 ± 0.053

mental colour (2 kpc radius $(g-z)$), while fitting for a mass step per bin. Doing so, β does not significantly vary, with $\Delta AIC = 0.2$ between a linear β -colour evolution and a fixed value.

We thus conclude from this detailed study of the standardisation parameters as a function of SN Ia environment that: (1) β depends on the host stellar mass, such that lower mass hosts ($\log(M_*/M_\odot) < 9.2$) exhibit a higher β than other targets. This low-mass host β value is compatible with expectation from dust model ($\beta \sim 4.1$) if the colour-magnitude relation is indeed driven by Milky Way-like dust. (2) Accounting for β variations does not cancel the mass step and/or the local colour step, which seems to play a significant role in SN Ia standardisation. The accurate modeling of SN Ia astrophysical dependencies thus seems more complicated than expected.

A different β for high/low mass host SNe has previously been seen in Sullivan et al. (2010); Rubin et al. (2015, 2023). González-Gaitán et al. (2021) find a 2.9 difference in β when fitting in two β bins, and no reduction of the mass step when fitting multiple (up to 4) β , in accordance with our results. In a companion paper, Popovic et al. (2024c) present a similar analysis including high redshift data and draw similar conclusions concerning the β -host mass relation that does not seem to vary as a function of redshift. In the next section we further investigate the Brout & Scolnic (2021) model, which suggests that β evolves as a function of host mass, and claims this is the root cause of the other astrophysical biases (see also Popovic et al. 2023; Wiseman et al. 2023).

5. Colour dependency of SN Ia standardised magnitudes (steps)

In this section, we investigate how the environmental step depends on SN colour. In Brout & Scolnic (2021), the origin of the residual SN Ia magnitude environmental step has been modeled as variations of the dust content (related to c) and properties (related to β) as a function of the host stellar mass. In Sect. 3, we confirm that indeed the colour distribution seems twofold, with redder SNe Ia getting their colour excess from host dependent properties and likely from interstellar dust.

To test for the hypothesis of the dust origin of the steps, one can compute steps for different colour bins. If dust is the main driver of the observed magnitude step, bluer SNe (i.e. not reddened by dust) should not exhibit a step. On the contrary, for red SNe, a step should appear, signalling two different colour-correcting laws (i.e. two β) for the two different environments. The hypothesis of the existence of different β for different host environments has been challenged in Sect. 4.1, but not as a function of SN colour.

A first simple test for the dust hypothesis for the step origin is to cut our sample in two on SN colour, and to compute steps separately. The values of blue ($c < 0$, 373 SNe) and red ($c > 0$,

Table 3. Parameters of the step evolution with SN colour: slope of the fit and ΔAIC between an affine function and a constant.

Tracer	Slope	ΔAIC
$(g - z)_{\text{local}}$	$0.08 \pm 0.12 (0.7\sigma)$	1.6
$(g - z)_{\text{global}}$	$0.08 \pm 0.12 (0.7\sigma)$	1.6
$\log(M_{\star}/M_{\odot})_{\text{local}}$	$0.02 \pm 0.14 (0.2\sigma)$	2.0
$\log(M_{\star}/M_{\odot})_{\text{global}}$	$0.01 \pm 0.12 (0.1\sigma)$	2.0

547 SNe) steps are compiled in Table 2. All of the blue SN steps are significantly different from 0. The red SNe mass steps are larger than the blue ones, but still consistent with the blue steps. The blue local colour steps are however slightly larger than the red local colour steps. This points towards dust not accounting for the whole environmental step.

We then focus on replicating Fig. 6 of Brout & Scolnic (2021), as was also done in Kelsey et al. (2023); Popovic et al. (2023); Wiseman et al. (2023). We thus plot in Fig. 7 the corrected Hubble residuals, magnitude step and scatter split on environment as a function of SN colour. Unlike Brout & Scolnic (2021), but as was done in Kelsey et al. (2023), we consider local and global colour ($g - z$) as well as local stellar mass as environment tracers, in addition of global stellar mass.

It is clearly noticeable in the top plots of Fig. 7 that locally blue environments/low mass host SNe Ia are significantly fainter than locally red environments/high mass host SNe Ia, as expected given the measured local colour/global mass steps. We highlight that the upwards tilt of the Hubble residuals at low c is a direct consequence of the errors on c and not a sign of a colour dependent β . This is explained in more detail in Appendix A. However, unlike Brout & Scolnic (2021), we do not observe any SN colour dependency in the shape of the residuals. The step amplitudes and scatter are also consistent across all colour bins.

To quantify the deviation of the steps from a constant (middle plot of Fig. 7), we fit for both a constant and an affine function on the steps-SN colour relation. The values for the slope of the fit and the ΔAIC between a constant and an affine fit for each of the tracers are presented in Table 3. All slopes of the steps-colour relation are less than 1σ away from zero, and for all tracers the difference in AIC between a constant and an affine function is lower than 2, making the evolution of the step with colour not supported. These conclusions stand when using Hubble residuals standardised with the broken- α from Ginolin et al. (2024a). The results also remain the same when reducing the number of bins.

Finally, we plot the scatter (normalised median absolute deviation, nmad) of the residuals for SNe in different environments in the bottom plots of Fig. 7. We do see a slight increase in the scatter for redder SNe, which might indicate a higher dust content, as dust not only dims but also scatters SN magnitudes. However, we do not see a difference in scatter between SNe in different environments, as was seen in Brout & Scolnic (2021) for SNe in high/low mass hosts. This was also not replicated by any of the following analyses (Wiseman et al. 2022; Kelsey et al. 2023).

6. Discussion

6.1. Tests

To assess the robustness of our results, we test the impact of the choices made in Sect. 2 on our results, namely the difference of dust content τ between the full sample and the dustless sample,

Test	Sample Size	$\Delta\tau$ [σ]	$\Delta\text{AIC}_{\beta \text{ evol}}$	Slope [σ]
Main analysis	927	4.6	4.2	2.5
$z_{\text{max}} = 0.05$	607	4.2	0.6	1.2
$z_{\text{max}} = 0.07$	1316	5.5	6.8	3.0
Host z	698	4.5	0.2	1.4
incl. Ia-pec	946	4.4	0.9	1.1
discard 91t	864	4.1	1.1	1.8
$c < 0.3$	834	2.0	3.0	2.5
$\chi^2_{\text{SALT}} < 0.1$	723	4.1	7.3	3.1

Table 4. Sample size, difference in τ_{dust} between the full sample and the dustless sample, ΔAIC between a constant and an affine function fitted on the β evolution with mass and significance of the slope of this affine function, for the different test samples described in Sect. 6.1.

and the significance of the β evolution (here the ΔAIC between a constant fit and an affine function fit of the β -global mass relation as well as the significance of the slope in σ). The tests on the β evolution are made using a linear correction in stretch α . The different tests made are:

- Changing our redshift cut: lowering z_{max} strengthen the volume-limited claims, while increasing z_{max} increases the statistics with a limited bias in the sample.
- Only using redshifts from host spectra allows for a test of the impact of redshift errors on the sample.
- Classification: including peculiar SNe Ia mimics the contamination that could happen when only using photometric classification, and discarding 91t allows us to check that our results do not depend on this subpopulation.
- Using a stronger cut on colour ($c < 0.3$), to check that our results are not reliant on redder objects.
- Enforcing a stronger cut on lightcurve fit quality ensures that our results are not due to poorly fitted objects.

For the β evolution analysis, the bins are fixed throughout the tests to get a fair comparison.

The results for each test are presented in Table 4. We see a slight reduction of the significance of our results when using $z_{\text{max}} = 0.05$, probably due to the lower statistics. On the other hand, the statistical boost of going to $z_{\text{max}} = 0.07$ increases the significance of $\Delta\tau_{\text{dust}}$ as well as the β evolution. Using only host redshifts drastically lowers the β evolution significance. This is likely due to the different host mass distributions described in Ginolin et al. (2024a). Indeed, the host- z sample probes higher masses than the full sample, as it is easier to get a galaxy spectrum for massive galaxies. Thus, the low-mass bin of the β evolution analysis is underfilled, and the resulting β has a very high errorbar, while its value is consistent with the full sample. Including peculiar SNe Ia does not affect the dust analysis but the significance of the β evolution decreases. This is due to a lower β in the lowest mass bin. This might be a statistical fluctuation, as this change only adds 19 objects to the sample. Discarding 91t does not affect $\Delta\tau$, but reduces the significance of the β evolution. This is due to the β value in second-lowest mass bin, which is lower than for the full sample. Only using $c < 0.3$ SNe strongly reduces the significance of $\Delta\tau$. This is expected, as τ is mostly constrained by the red tail of the colour distribution. However, the β evolution tests are similar, in accordance with the conclusion of Sect. 4.1 that β is the same for the full colour

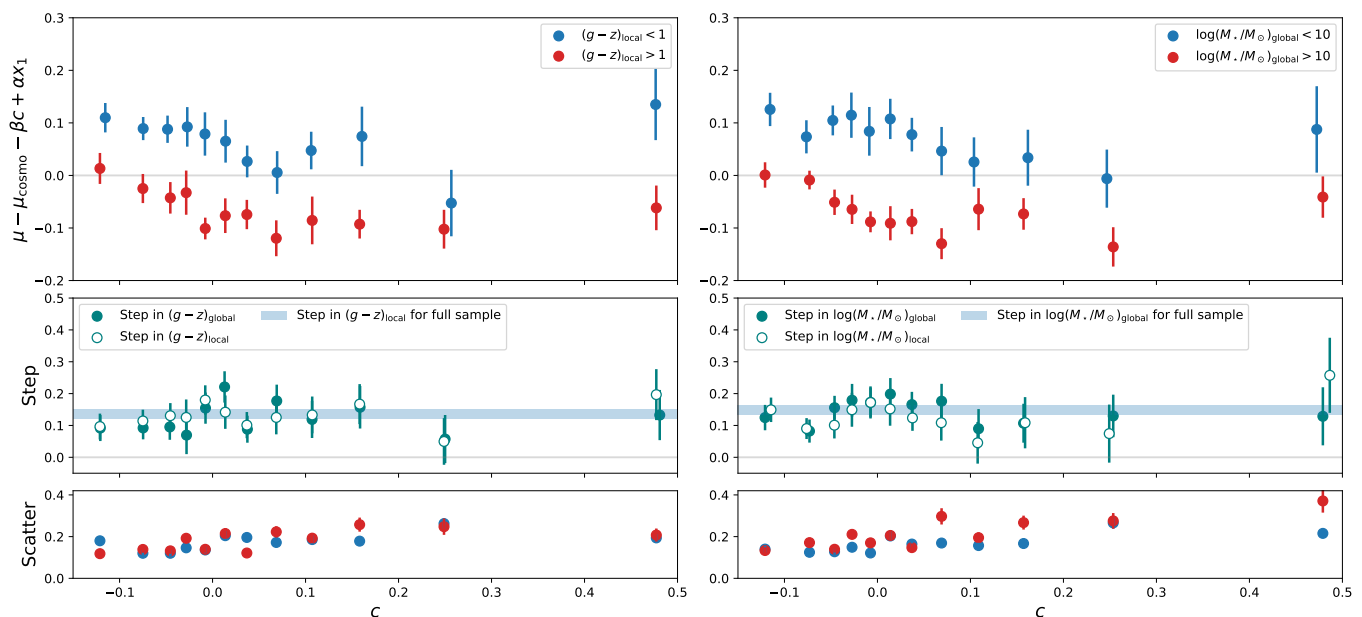


Fig. 7. *Top:* Binned Hubble residuals versus SNe colour, split on local colour (left) and global mass (right). There are ~ 80 SNe in each bin. *Middle:* Steps computed for each colour bin, with a split on global and local colour (left) or mass (right). *Bottom:* Residuals scatter for each colour bins, for locally blue/red (left) or globally low mass/high mass (right) environments.

range. Enforcing a stricter cut on χ^2_{SALT2} gives a stronger β evolution, as the errorbar on the low-mass bin is reduced compared to the full sample case. This might be due to smaller errors on c on average, due to a better SALT2.4 fit.

6.2. Dust in galaxies

The τ parameter from Eq. 1 can inform us on the dust content of the SN environments, as seen in Fig. 2. The decline of extinction for both elliptical and spiral galaxies, and for different mass ranges, is studied in Goddard et al. (2017); González Delgado et al. (2015); Battisti et al. (2016). As expected, the outskirts of galaxies (i.e. high dDLR regions) are less dusty than galaxy cores, for both early and late type galaxies, even if the slope of the extinction-radius relation is greater for late types. Following the known stellar mass/dust mass relation (Beeston et al. 2018), massive spiral galaxies have more dust than low-mass galaxies at a given radius. This is not visible for elliptical galaxies due to the relatively flat shape of the extinction-radius relation. Because red environments are also more massive, we expect red environments to be more dusty (Lange et al. 2015). Those relations hold for global parameters.

For spiral galaxies, Smith et al. (2016) show that the distribution of dust is consistent with an exponential decay with a gradient of $\sim -1.7 \text{ dex } R_{25}^{-1}$ (with R_{25} the radius where the optical brightness corresponds to a B-band brightness of 25 mag arcsec $^{-2}$, Bigiel & Blitz 2012). They further show that such a decline is very alike that of stellar density, which is slower than that of star formation rate surface density. This hints at a stronger relation between local stellar mass and dust than for local colour.

Overall, studies of the dust content in galaxies agree well with the conclusions from Fig. 2.

7. Conclusion

This paper presents an analysis of the colour term of the standardisation procedure used in SN Ia cosmology, as well as its dependence on environment and its link to environmental magnitude offsets (steps). A companion paper (Ginolin et al. 2024a) focuses on stretch and steps. We make use of the volume-limited version of the ZTF DR2 SN Ia sample, a sample of 927 SNe Ia. This sample is free from selection effects, which allows us to study true underlying distributions and correlations without any biases.

Our conclusions are the following:

- We probe SN colour up to $c = 0.8$. Its distribution is well characterised by the convolution of a Gaussian (thought to be the intrinsic colour distribution) and an exponential tail (thought to be host galaxy dust reddening).
- Using environmental cuts to isolate non-dusty environments (large dDLR and locally low stellar mass environments), we observe a significant reduction of the red exponential tail (4.6σ), suggesting that indeed this term accounts for extra dust reddening that dominates SN colour at $c > 0.2$.
- Looking at the colour-residuals relation, a linear β along the full SN colour range ($-0.2 < c < 0.8$) matches surprisingly well the data. We see for instance no deviations near $c \sim 0.2$, suggesting that, whatever the cause of the SN colour is, the colour-magnitude relation seems colour-independent.
- We however see hints of an evolution of the colour-residuals relation slope β with the host galaxy stellar mass, with the slope being only 2.5σ away from zero. We find SNe in massive host to have lower β values. When accounting for the broken-alpha standardisation found in Ginolin et al. (2024a), the slope remains at the 2.3σ level.
- Finally, we see no dependency of the amplitude of the environmental magnitude offset γ as a function of SN colour, unlike recent results from the literature (e.g., Brout & Scolnic 2021; Kelsey et al. 2023). This suggests that the host interstellar dust may not be the parameter driving the observed magnitude offsets.

Acknowledgements. Based on observations obtained with the Samuel Oschin Telescope 48-inch and the 60-inch Telescope at the Palomar Observatory as part of the Zwicky Transient Facility project. ZTF is supported by the National Science Foundation under Grants No. AST-1440341 and AST-2034437 and a collaboration including current partners Caltech, IPAC, the Weizmann Institute of Science, the Oskar Klein Center at Stockholm University, the University of Maryland, Deutsches Elektronen-Synchrotron and Humboldt University, the TANGO Consortium of Taiwan, the University of Wisconsin at Milwaukee, Trinity College Dublin, Lawrence Livermore National Laboratories, IN2P3, University of Warwick, Ruhr University Bochum, Northwestern University and former partners the University of Washington, Los Alamos National Laboratories, and Lawrence Berkeley National Laboratories. Operations are conducted by COO, IPAC, and UW. SED Machine is based upon work supported by the National Science Foundation under Grant No. 1106171. The ZTF forced-photometry service was funded under the Heising-Simons Foundation grant #12540303 (PI: Graham). This project has received funding from the European Research Council (ERC) under the European Union's Horizon 2020 research and innovation program (grant agreement n 759194 - USNAC). This work has been supported by the Agence Nationale de la Recherche of the French government through the program ANR-21-CE31-0016-03. This work was supported by the GROWTH project (Kasliwal et al. 2019) funded by the National Science Foundation under Grant No 1545949. TEMB acknowledges financial support from the Spanish Ministerio de Ciencia e Innovación (MCIN), the Agencia Estatal de Investigación (AEI) 10.13039/501100011033, and the European Union Next Generation EU/PRTR funds under the 2021 Juan de la Cierva program FJC2021-047124-I and the PID2020-115253GA-I00 HOST-FLOWS project, from Centro Superior de Investigaciones Científicas (CSIC) under the PIE project 20215AT016, and the program Unidad de Excelencia María de Maeztu CEX2020-001058-M. LG acknowledges financial support from AGAUR, CSIC, MCIN and AEI 10.13039/501100011033 under projects PID2020-115253GA-I00, PIE 20215AT016, CEX2020-001058-M, and 2021-SGR-01270. UB, JHT, MD, GD and KM are supported by the H2020 European Research Council grant no. 758638. This work has been supported by the research project grant "Understanding the Dynamic Universe" funded by the Knut and Alice Wallenberg Foundation under Dnr KAW 2018.0067, *Vetenskapsrådet*, the Swedish Research Council, project 2020-03444. Y.-L.K. has received funding from the Science and Technology Facilities Council [grant number ST/V000713/1]. SD acknowledges support from the Marie Curie Individual Fellowship under grant ID 890695 and a Junior Research Fellowship at Lucy Cavendish College.

References

Amanullah, R., Johansson, J., Goobar, A., et al. 2015, *MNRAS*, 453, 3300
 Barone-Nugent, R. L., Lidman, C., Wyithe, J. S. B., et al. 2012, *MNRAS*, 425, 1007
 Battisti, A. J., Calzetti, D., & Chary, R. R. 2016, *ApJ*, 818, 13
 Beeston, R. A., Wright, A. H., Maddox, S., et al. 2018, *MNRAS*, 479, 1077
 Bellm, E. C., Kulkarni, S. R., Graham, M. J., et al. 2019, *PASP*, 131, 018002
 Betoule, M., Kessler, R., Guy, J., et al. 2014, *A&A*, 568, A22
 Bigiel, F. & Blitz, L. 2012, *ApJ*, 756, 183
 Briday, M., Rigault, M., Graziani, R., et al. 2021, *A&A*, 657, A22
 Brout, D. & Scolnic, D. 2021, *ApJ*, 909, 26
 Brout, D., Taylor, G., Scolnic, D., et al. 2021, arXiv e-prints, arXiv:2112.03864
 Burnham, K. P. & Anderson, D. R. 2004, *Sociological Methods & Research*, 33, 261
 Chambers, K. C., Magnier, E. A., Metcalfe, N., et al. 2016, arXiv e-prints, arXiv:1612.05560
 Childress, M., Aldering, G., Antilogus, P., et al. 2013, *ApJ*, 770, 108
 Dekany, R., Smith, R. M., Riddle, R., et al. 2020, *PASP*, 132, 038001
 Dembinski, H. & et al., P. O. 2020
 Dhawan, S., Jha, S. W., & Leibundgut, B. 2018, *A&A*, 609, A72
 Freedman, W. L. 2021, *ApJ*, 919, 16
 Galbany, L., de Jaeger, T., Riess, A. G., et al. 2022, arXiv e-prints, arXiv:2209.02546
 Galbany, L., Miquel, R., Östman, L., et al. 2012, *ApJ*, 755, 125
 Goddard, D., Thomas, D., Maraston, C., et al. 2017, *MNRAS*, 466, 4731
 González Delgado, R. M., García-Benito, R., Pérez, E., et al. 2015, *A&A*, 581, A103
 González-Gaitán, S., de Jaeger, T., Galbany, L., et al. 2021, *MNRAS*, 508, 4656
 Goobar, A. 2008, *ApJ*, 686, L103
 Graham, M. J., Kulkarni, S. R., Bellm, E. C., et al. 2019, *PASP*, 131, 078001
 Gupta, R. R., Kuhlmann, S., Kovacs, E., et al. 2016, *AJ*, 152, 154
 Guy, J., Sullivan, M., Conley, A., et al. 2010, *A&A*, 523, A7
 Hamuy, M., Phillips, M. M., Suntzeff, N. B., et al. 1996, *AJ*, 112, 2391
 Jha, S., Riess, A. G., & Kirshner, R. P. 2007, *ApJ*, 659, 122
 Johansson, J., Cenko, S. B., Fox, O. D., et al. 2021, *ApJ*, 923, 237

Jones, D. O., Mandel, K. S., Kirshner, R. P., et al. 2022, *ApJ*, 933, 172
 Kasliwal, M. M., Cannella, C., Bagdasaryan, A., et al. 2019, *PASP*, 131, 038003
 Kelly, P. L., Hicken, M., Burke, D. L., Mandel, K. S., & Kirshner, R. P. 2010, *ApJ*, 715, 743
 Kelsey, L., Sullivan, M., Smith, M., et al. 2021, *MNRAS*, 501, 4861
 Kelsey, L., Sullivan, M., Wiseman, P., et al. 2023, *MNRAS*, 519, 3046
 Kim, Y.-L., Smith, M., Sullivan, M., & Lee, Y.-W. 2018, *ApJ*, 854, 24
 Lampeitl, H., Smith, M., Nichol, R. C., et al. 2010, *ApJ*, 722, 566
 Lange, R., Driver, S. P., Robotham, A. S. G., et al. 2015, *MNRAS*, 447, 2603
 Maeda, K. & Terada, Y. 2016, *International Journal of Modern Physics D*, 25, 1630024
 Mandel, K. S., Narayan, G., & Kirshner, R. P. 2011, *ApJ*, 731, 120
 Mandel, K. S., Scolnic, D. M., Shariff, H., Foley, R. J., & Kirshner, R. P. 2017, *ApJ*, 842, 93
 Masci, F. J., Laher, R. R., Rusholme, B., et al. 2019, *PASP*, 131, 018003
 Nicolas, N., Rigault, M., Copin, Y., et al. 2021, *A&A*, 649, A74
 Nobili, S. & Goobar, A. 2008, *A&A*, 487, 19
 Perlmutter, S., Aldering, G., Goldhaber, G., et al. 1999, *ApJ*, 517, 565
 Phillips, M. M. 1993, *ApJ*, 413, L105
 Planck Collaboration. 2020, *A&A*, 641, A6
 Ponder, K. A., Wood-Vasey, W. M., Weyant, A., et al. 2021, *ApJ*, 923, 197
 Popovic, B., Brout, D., Kessler, R., & Scolnic, D. 2021, arXiv e-prints, arXiv:2112.04456
 Popovic, B., Brout, D., Kessler, R., & Scolnic, D. 2023, *ApJ*, 945, 84
 Riess, A. G., Filippenko, A. V., Challis, P., et al. 1998, *AJ*, 116, 1009
 Riess, A. G., Yuan, W., Macri, L. M., et al. 2022, *ApJ*, 934, L7
 Rigault, M., Brinnet, V., Aldering, G., et al. 2020, *A&A*, 644, A176
 Rigault, M., Copin, Y., Aldering, G., et al. 2013, *A&A*, 560, A66
 Roman, M., Hardin, D., Betoule, M., et al. 2018, *A&A*, 615, A68
 Rose, B. M., Popovic, B., Scolnic, D., & Brout, D. 2022, *MNRAS*, 516, 4822
 Rubin, D., Aldering, G., Barbary, K., et al. 2015, *ApJ*, 813, 137
 Rubin, D., Aldering, G., Betoule, M., et al. 2023, arXiv e-prints, arXiv:2311.12098
 Salim, S., Boquien, M., & Lee, J. C. 2018, *ApJ*, 859, 11
 Scolnic, D. M., Jones, D. O., Rest, A., et al. 2018, *ApJ*, 859, 101
 Smith, M. W. L., Eales, S. A., De Looze, I., et al. 2016, *MNRAS*, 462, 331
 Sullivan, M., Conley, A., Howell, D. A., et al. 2010, *MNRAS*, 406, 782
 Sullivan, M., Le Borgne, D., Pritchett, C. J., et al. 2006, *ApJ*, 648, 868
 Taylor, G., Lidman, C., Tucker, B. E., et al. 2021, *MNRAS*, 504, 4111
 Tripp, R. 1998, *A&A*, 331, 815
 Uddin, S. A., Burns, C. R., Phillips, M. M., et al. 2020, *ApJ*, 901, 143
 Wang, L. 2005, *ApJ*, 635, L33
 Wiseman, P., Sullivan, M., Smith, M., & Popovic, B. 2023, *MNRAS*, 520, 6214
 Wiseman, P., Vincenzi, M., Sullivan, M., et al. 2022, *MNRAS*, 515, 4587

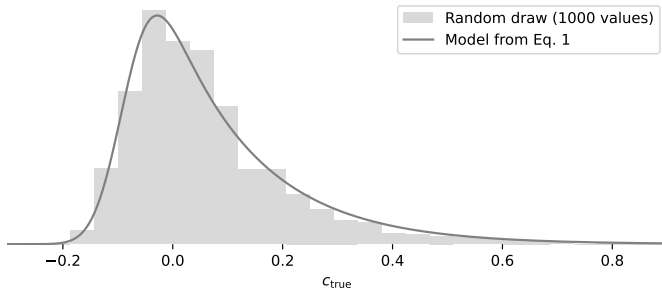


Fig. A.1. Histogram of the 1,000 colour values simulated using the colour model from Eq. 1 with values from the full sample in Table 1 (grey line).

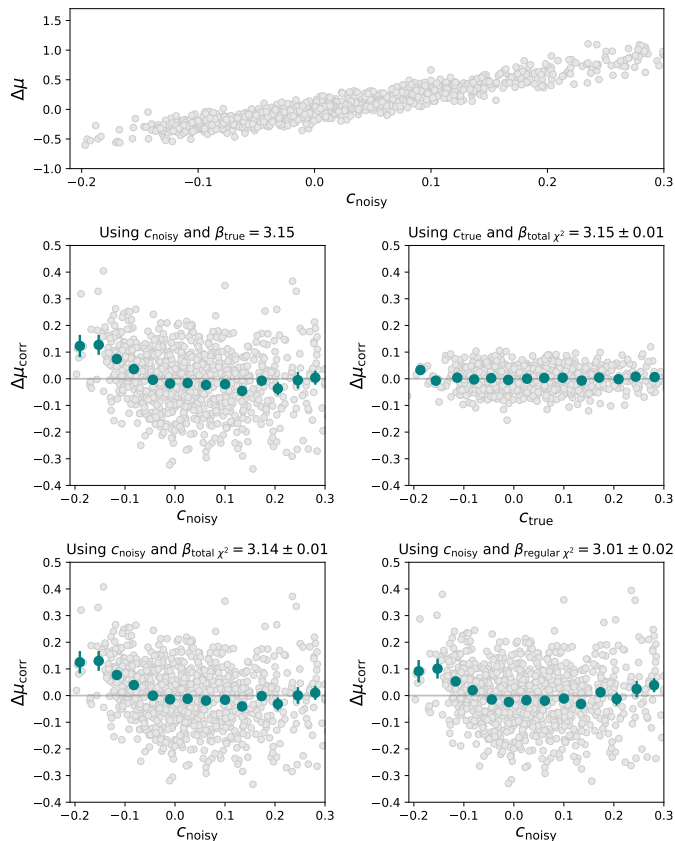


Fig. A.2. *Top:* Simple simulation of noisy residuals with a correlation with colour β . *Middle left:* Residuals corrected for their correlation with colour with the true correlation coefficient β but noisy colours c_{noisy} . An upwards tilt appears at low colours due to errors on c_{noisy} . *Middle right:* Residuals corrected for their correlation with colour with the true correlation coefficient β and true colours c_{true} . The corrected residuals appear flat with colour. *Bottom right:* Residuals corrected with an unbiased β fitted with the total- χ^2 method. *Bottom left:* Residuals corrected with a biased β fitted with the regular χ^2 minimisation.

Appendix A: Shape of the colour-residuals relation

In this Appendix, we discuss the shape of the colour and stretch corrected residuals in Fig. 7, in particular the upwards tilt of the residuals seen at lower colours. This discussion can apply for any fit of a linear relation between two noisy variables. We here only demonstrate the principle of this effect on a simple case, with a single linear relation between residuals and colour, not accounting for stretch and environment correlations, and without intrinsic

scatter. We simulate a colour sample (1,000 objects) using the model from Eq. 1 and the parameters from the full sample fit presented in Table 1. The histogram of those colour values along with the distribution used to generate them are plotted in Fig. A.1. We then apply Gaussian noise on the true colour values c_{true} to get noisy colour values $c_{\text{noisy}} = c_{\text{true}} + \mathcal{N}(0, \sigma_c)$, where $\sigma_c = 0.035$ is roughly the mean error on colour in our data. On the other hand, we compute noisy residuals, only adding a correlation with colour, so that $\Delta\mu = \beta_{\text{true}}c_{\text{true}} + \mathcal{N}(0, \sigma_\mu)$, with $\beta_{\text{true}} = 3.15$. $\sigma_\mu = 0.04$ is the typical measurement error on magnitudes in our data. These noisy residuals are plotted against noisy colour in the top plot of Fig. A.2.

We finally compute corrected residuals. We first use the true β and the noisy colour to correct for the colour-residuals correlation, such that $\Delta\mu_{\text{corr}} = \Delta\mu - \beta_{\text{true}}c_{\text{noisy}}$. This is plotted in the middle left plot of Fig. A.2. We can see the upwards tilt at low colour appear, even though we corrected with the true β . We also compute the residuals corrected with the true colours, $\Delta\mu_{\text{corr}} = \Delta\mu - \beta_{\text{true}}c_{\text{true}}$, presented in the middle right plot of Fig. A.2. In that case, the residuals appear flat with colour. We thus illustrate that the upwards tilt of the colour-residuals relation seen in Fig. 7 is not the consequence of a colour-dependent β . The magnitude of this effect is stronger when errors on the x variable (here c) are bigger.

Errors on the y -axis on the fit are the reason why a regular χ^2 optimisation algorithm is biased in β (as well as α and γ when considering the full standardisation process), so that we need to use a total- χ^2 fitting method to get unbiased standardisation parameters. The total- χ^2 method fits for the "true" x variables (in our case c) as latent parameters. This is illustrated in the bottom plots of Fig. A.2. Indeed, on the bottom left plot are residuals corrected with noisy colours and β fitted with the total- χ^2 algorithm used throughout this paper. We find here $\beta_{\text{total } \chi^2} = 3.14 \pm 0.01$, close to the input value $\beta_{\text{true}} = 3.15$. On the bottom right plot of Fig. A.2 are the residuals corrected with noisy colours and β fitted with the usual χ^2 algorithm. We find $\beta_{\text{regular } \chi^2} = 3.01 \pm 0.02$, a 6.9σ bias. The lower β is trying to compensate for the tilt seen at low colour. A detailed explanation of the total- χ^2 fitting method can be found in Section 4.2 of [Ginolin et al 2024a](#), as well as a more thorough investigation of biases on fitted standardisation parameters using realistic ZTF sample simulations in Appendix A.